第 41 卷 第 2 期
2020 年 2 月
焊 接 学 报
TRANSACTIONS OF THE CHINA WELDING INSTITUTION
Vol. 41(2):33 − 38
February 2020

超声电弧对 6061 铝合金 MIG 焊接头组织和性能的影响

雷玉成[1]， 崔展祥[1]， 路广遥[2]， 姚亦强[2]， 张雪宁[1]
(1. 江苏大学, 镇江, 212013; 2. 中广核研究院有限公司, 深圳, 518000)

摘要: 为了改善铝合金 MIG 焊的接头质量, 利用外接超声激励装置在 MIG 焊接电弧中激发出超声, 并研究了超声激励频率对 6061 铝合金对接焊缝的成形、气孔分布、显微组织及力学性能的影响规律. 结果表明, 超声电弧可以有效的细化焊缝组织、减少焊缝气孔量, 提升接头的强度. 与常规 MIG 焊接相比, 在引入超声电弧后, 焊缝的熔宽增加, 焊缝中胞状树枝晶组织被细化, 等轴晶区域占比增加, 在激励频率为 30 kHz 时组织细化效果最好; 随着激励频率的增加, 焊缝中的气孔量逐渐降低, 焊接接头的抗拉强度提高, 当激励频率为 50 kHz 时, 抗拉强度最高, 达到 235 MPa, 为母材强度的 73.4%, 对应拉伸断口中韧窝的形态更加等轴化、分布更加均匀.

关键词: 超声电弧; 激励频率; 显微组织; 抗拉强度; 6061 铝合金
中图分类号: TG444, TG402　　**文献标识码:** A　　**doi:** 10.12073/j.hjxb.20191006002

0 序言

车辆制造产业中, 轻量化是一个发展方向. 铝合金的密度小、比强度高、耐蚀性好、工艺性能好, 已经成为车身结构轻量化的关键材料之一[1], 而实现铝合金的高质量焊接是车身轻量化的重要保障.

MIG 焊、TIG 焊因为设备简单、工艺成熟, 是铝合金车身常用的焊接方法[2]. 目前 6061 铝合金焊接接头仍存在气孔、组织粗大、软化的问题. 超声电弧焊接是近年来出现的一种复合焊接技术[3-4], 与一般的机械复合[5-6] 方法不同, 它将超声频电信号直接加进电弧中, 以改善焊接质量, 有学者发现对碳钢、合金钢、钛合金、复合材料等材料来说, 这种方法对接头有细化晶粒、除气、提升力学性能的作用[7-8], 所以超声电弧焊接有望解决 6061 铝合金的焊接缺陷问题.

试验中通过接入超声波激励电源, 对 MIG 焊接电弧进行高频调制, 激发出超声电弧, 对 6061 铝合金板材进行超声电弧-MIG 自动化焊接, 来研究超声电弧的引入对于接头的成形、气孔量、显微组织、抗拉强度及断后伸长率的影响.

收稿日期: 2019 − 10 − 06
基金项目: 国家自然科学基金资助项目 (51875264)

1 试验方法

1.1 超声电弧-MIG 焊接试验系统

在超声电弧-MIG 焊接系统中, 使用自制的隔离耦合装置, 使 MIG 直流焊接电源和超声激励电源实现电气连接, 该装置在不同的激励频率下搭配不同电气参数的元器件, 以增大激励源的传输效率, 减小电弧负载上的信号失真. 超声激励源的电压和频率均可调, 激励电压调节范围为 0 ~ 170 V, 激励频率调节范围为 20 ~ 100 kHz, 图 1 为超声电弧 MIG 焊接系统的原理图.

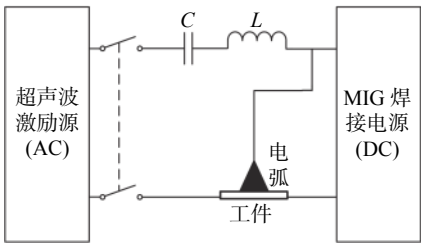

图 1 超声电弧-MIG 焊接系统原理示意图
Fig. 1 Schematic of arc-ultrasonic welding system

1.2 试验材料和方法

试验所用材料为 6061-T6 铝合金, 化学成分如表 1 所示. 焊接所用填充材料为直径 1.2 mm 的 ER5356 焊丝, 其合金成分如表 2 所示.

表 1 6061-T6 铝合金化学成分 (质量分数，%)
Table 1 Chemical compositions of 6061-T6 aluminum alloy

Cu	Mn	Mg	Zn	Cr	Ti	Si	Fe	Al
0.2	0.26	0.83	0.03	0.04	0.02	0.8	0.29	余量

表 2 ER5356 焊丝化学成分 (质量分数，%)
Table 2 Chemical compositions of ER5356 wire

Mn	Mg	Cr	Ti	Al
0.1	4.8	0.08	0.1	余量

将 6061-T6 铝板加工成 140 mm × 70 mm × 4 mm 的板材，焊接前用钢丝球把试板的待焊接面打磨干净，并用丙酮清洗表面的污渍. 用奥太 Pulse MIG-350Y 焊机对处理好的铝板进行对接焊接，不开坡口，背部加带有 2 mm 深弧形槽的铜垫板，保护气为纯度 99.99% 的氩气. 常规的 MIG 焊使用的焊接参数如表 3 所示. 试验时，采用正常的直流反接极性，待正常 MIG 焊接电弧稳定时，打开隔离耦合装置开关，使超声激励信号接入. 选定电弧两极的超声激励电压 U_b 为 40 V 不变，波形如图 2 所示，激励频率 f 为 30, 50, 70, 85 kHz.

表 3 MIG 焊接参数及超声激励参数
Table 3 Parameters of MIG welding and ultrasonic excitation

焊接电压 U/V	焊接电流 I/A	焊接速度 v/(mm·min^{-1})	氩气流量 q/(L·min^{-1})	激励频率 f/kHz
22.7	190	800	15	30/50/70/85

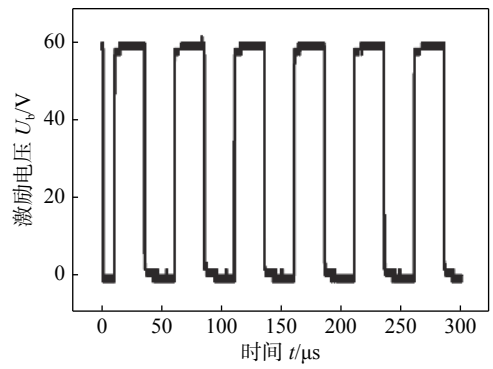

图 2 激励频率为 20 kHz 时超声电源的输出信号
Fig. 2 Output signal image of ultrasonic power supply with excitation frequency of 20 kHz

焊接完成后，沿垂直于焊缝的方向截取试样，用 Nikon SMZ25 体式显微镜对焊缝形貌、焊缝气孔的形态和分布进行观察. 沿平行于焊缝方向取样，用 Zeiss 金相显微镜对焊缝组织形貌进行观察. 在 DDL100 电子万能试验机上进行拉伸试验，拉伸速度为 2 mm/min，并用 NovaNano450 扫描电子显微镜观察断口形貌.

2 试验结果与分析

2.1 超声电弧对于焊缝成形的影响

试验中，与常规 MIG 焊接相比，超声电弧的加入没有改变 MIG 焊接电源输出的电流、电压，另外也通过声场检测设备确认了受激超声电弧的存在. 因为文中的试验保证接头熔透，背面强制成形，所以熔深不作考虑. 焊缝中不同位置的熔宽变化趋势不同，图 3 为不同激励频率下的焊缝截面形貌，白色横线为焊缝上表面、1/2 板厚处和背面的熔宽示意线，由此得到不同激励频率、不同焊缝位置的熔宽值变化曲线，如图 4 所示.

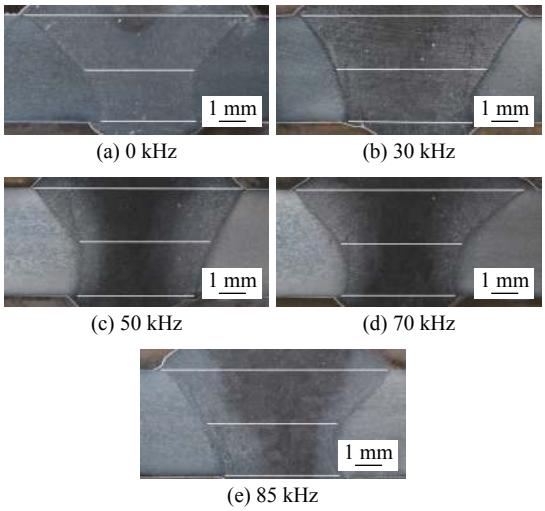

图 3 不同激励频率下接头的横截面形貌
Fig. 3 Weld cross-section appearance with different excitation frequencies. (a) 0 kHz; (b) 30 kHz; (c) 50 kHz; (d) 70 kHz; (e) 85 kHz

由图 3 可以看出，一般定义中的焊缝宽度，即焊缝的上表面熔宽，在加入超声电弧前后，是处在一个波动范围内的，波动幅度不大，除了频率为 50 kHz 时熔宽略有降低，其它频率下的熔宽都略有增加.

焊缝 1/2 板厚处熔宽和背面的熔宽有着相同的变化趋势，超声电弧的引入，使其熔宽值都有了明显的增加，其中在激励频率为 30 kHz 时，熔宽的增

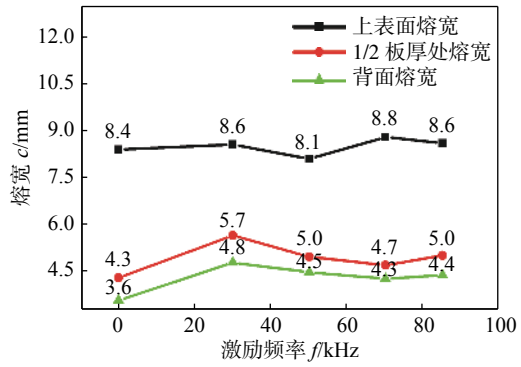

图 4　不同激励频率下焊缝不同位置的熔宽变化曲线

Fig. 4　Weld width curves of different parts of weld at different excitation frequencies

加最多. 因为在焊接过程中，熔合线属于固液交界面，超声在此处具有较强的振荡作用，在这个半熔化区中，超声的振动能量和声流效应[9] 会把结合不牢的结晶晶体打断并分散到液相中，扩展熔化边界，从试验结果来看，超声的振荡作用在焊缝中下部的熔合区作用更强. 另外超声的声流效应能促进流体的对流传热作用，使焊缝的中下部得到更多的热量，也能促进熔宽的增加.

2.2　超声电弧对焊缝气孔的影响

在未加超声电弧的常规 MIG 焊接中，6061 铝合金焊缝中弥散的分布着一定数量的气孔，如图 5 所示，这些气孔在焊缝上部分布居多，尺寸可达到微米级别，越靠近表面气孔越多，最大尺寸可达到 0.1 mm. 图 6 为施加不同频率的超声电弧后 MIG 焊焊缝的气孔分布图. 当超声激励频率为 30 kHz 时，焊缝的中部和上部仍弥散的分布着较多的气孔. 当激励频率增加到 50 和 70 kHz 时，焊缝中气孔的数量明显减少，气孔尺寸比 30 kHz 时的稍大，分布在焊缝的上部，表明在凝固前熔池中的气泡具有了“合并”和“长大”的倾向，而气泡尺寸越大，上浮速度就越大，越利于气体的排出. 当激励频率为 85 kHz 时，焊缝中气孔数量最少，尺寸细小，优化效果显著.

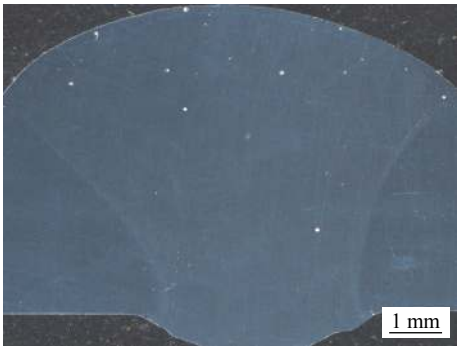

图 5　未加入超声电弧时焊缝的气孔分布

Fig. 5　Porosity distribution of weld without arc-ultrasonic treatment

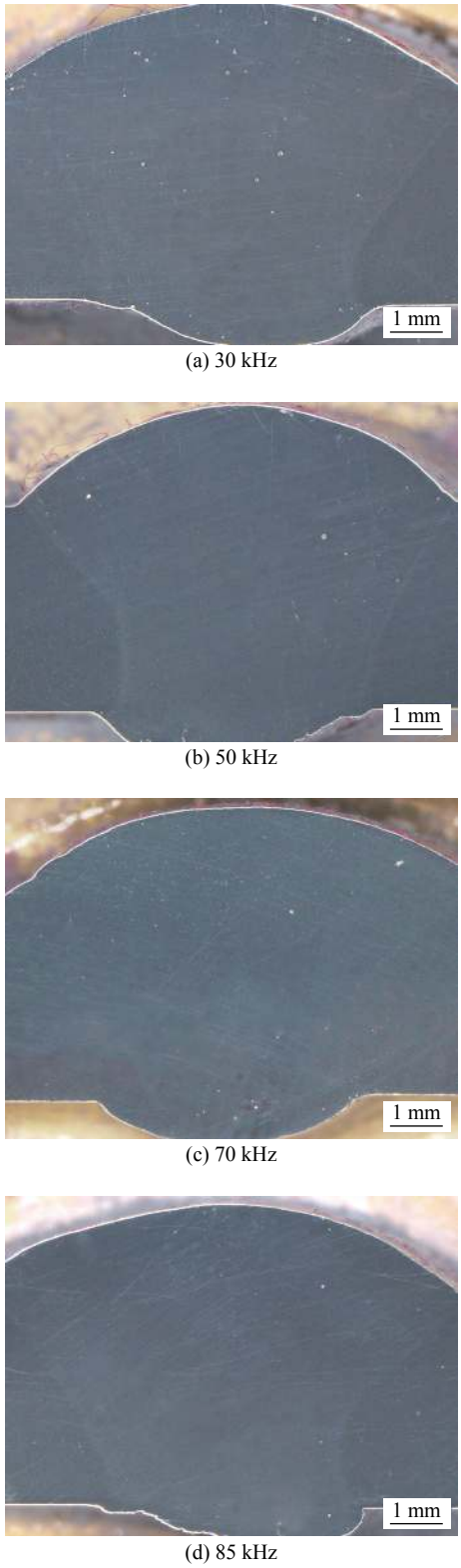

(a) 30 kHz

(b) 50 kHz

(c) 70 kHz

(d) 85 kHz

图 6　施加不同频率的超声电弧后焊缝气孔分布图

Fig. 6　Porosity distribution of weld with arc-ultrasonic treatment of different excitation frequencies. (a) 30 kHz; (b) 50 kHz; (c) 70 kHz; (d) 85 kHz

超声电弧的引入可以降低气孔数量，主要原因是超声的空化效应. 超声由电弧激发而传导至液态熔池，在熔池中形成大量的空化核，熔池中的气体因为压强差会向空化核释放和聚集，在超声的振动作用下移动、再次合并，进而浮出熔池. 同时，随着超声激励频率的增加，超声的空化效应变得更加剧烈，熔池中的气泡越容易合并长大，并从熔池中逸出.

2.3 超声电弧对焊缝显微组织的影响

在常规 MIG 焊接接头中，焊缝区晶粒尺寸和形态不均匀，如图 7 所示，中部组织主要由大量粗大的胞状树枝晶和少部分的等轴晶组成，单个胞状枝晶的尺寸可达 600 μm，枝晶中第二相间距较大，晶界处有偏析，越靠近焊缝上表面，枝晶组织越是发达.

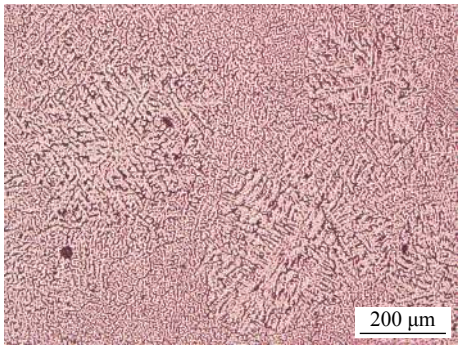

图 7 未加超声电弧时焊缝中部的微观组织

Fig. 7 Microstructure in the middle of the weld metal without arc-ultrasonic treatment

在加入不同激励频率的超声电弧后，焊缝区的晶粒有不同程度的变化，如图 8 所示，主要是粗大的胞状树枝晶数量减少、尺寸减小，等轴晶区域的面积增加. 在激励频率为 30 kHz 时，焊缝区组织中细小的等轴晶占主要组成部分，树枝晶的尺寸减小至 300 μm 左右，组织优化效果最好，50 kHz 时次之. 当激励频率为 70 kHz 时，焊缝中部组织出现了较多的柱状亚晶，如图 8c 所示. 激励频率为 85 kHz 时，等轴晶区域中大晶界较为明显. 可见，超声电弧的引入可以减少焊缝中部粗大树枝晶的数量，减小其尺寸，结合超声在液体中传播的相关效应可知，这些树枝晶在生长的过程中遭到了超声的“破碎”作用. 超声在液体介质中传播时产生强烈的冲击波[10]，这些冲击波可将正在生长的树枝状晶打碎和分散，减小其尺寸，而超声在黏性介质中的声流现象也会增加熔池的流动性，促进破碎晶核质点的分散和流动，使其成为新的形核质点，增加形核率，较低频的超声电弧处理更利于晶粒的细化.

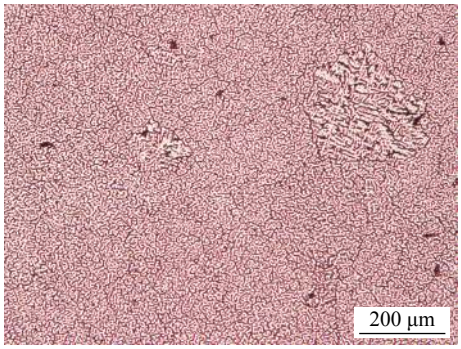

(a) 30 kHz

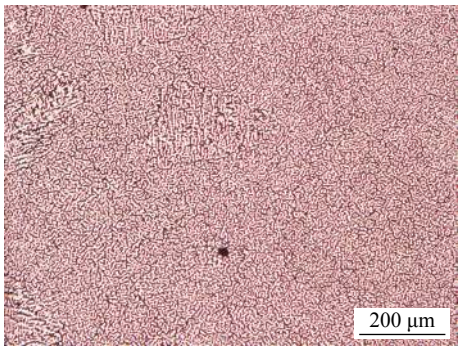

(b) 50 kHz

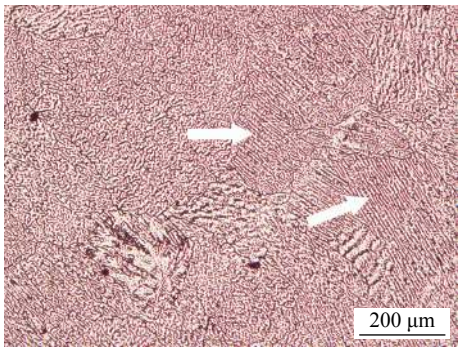

(c) 70 kHz

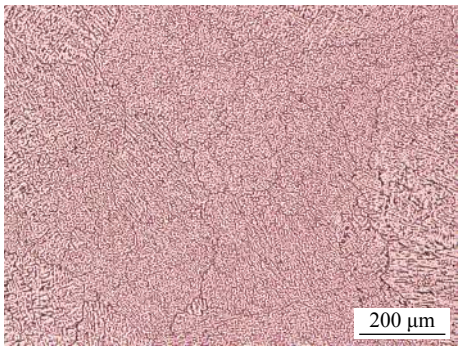

(d) 85 kHz

图 8 施加超声电弧后焊缝中部的微观组织

Fig. 8 Microstructure in the middle of the weld metal with arc-ultrasonic treatment. (a) 30 kHz; (b) 50 kHz; (c) 70 kHz; (d) 85 kHz

2.4 超声电弧对焊接接头力学性能的影响

对于常规的 MIG 焊和加入超声电弧的 MIG 焊，按照 GB/T228—2008 标准，在每种工艺参数的

接头上取 4 个试样进行常温拉伸试验. 试样的平均抗拉强度、平均断后伸长率如图 9所示. 常规的 MIG 焊接头的抗拉强度为214 MPa, 达到了母材强度的 66.8%. 加入超声电弧后, 抗拉强度和断后伸长率都有提高. 断后伸长率随激励频率增加而线性增加, 由 8% 最高提升到 13.3%. 激励频率为 50 kHz 时, 抗拉强度最高, 达到 235 MPa, 为母材的 73.4%, 比常规 MIG 焊接头增加 6.6%. 激励频率为 30 kHz 时, 抗拉强度提升较少.

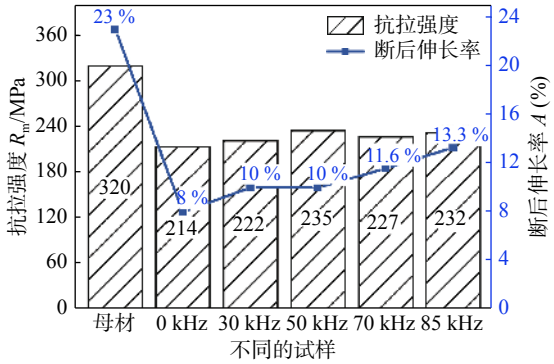

图 9　不同参数下接头的抗拉强度和断后伸长率

Fig. 9　Tensile strength and elongation of welded joints with different parameters

拉伸试样主要在焊缝区断裂, 部分在热影响区断裂, 少数在熔合区断裂, 断口边缘有不太完整的剪切唇, 微观断口具有韧窝形貌, 是典型的韧性断裂. 不同工艺参数下的接头的断口特征如图 10 所示, 图中白线代表焊缝熔合线的位置, 黑色箭头表示断裂位置, 根据断裂的位置和形貌断口类型可分为 4 类: Ⅰ型处于焊缝位置的剪切斜断口, 断口方向平行于最大切应力, 与拉伸主应力方向成 45°, 属于微孔聚集型断裂; Ⅱ型在焊缝的中部断面弯折, 与主应力方向仍保持近 45°, 属于微孔聚集型断裂, 伴随着裂纹源受力扩展的开裂, 断口弯折处是微裂纹发源处, 这里存在着较多的气孔、夹杂缺陷; Ⅲ型与Ⅰ型不同的是, 断口一侧经过熔合线, 是由于熔合区的柱状晶粒、气孔、偏析物集聚等缺陷使晶界结合强度变差, 只在常规 MIG 焊接头中少量出现; Ⅳ型微孔聚集型断裂, 在热影响区断裂, 断面不平直, 但仍与主应力方向呈近 45°, 这与铝合金过时效的组织特点有关.

在常规的 MIG 焊接头中, 断口类型主要为Ⅰ型、Ⅲ型, 焊缝组织主要由尺寸不均且粗大的胞状枝晶组成, 加上气孔、未熔合孔洞的缺陷, 使得焊

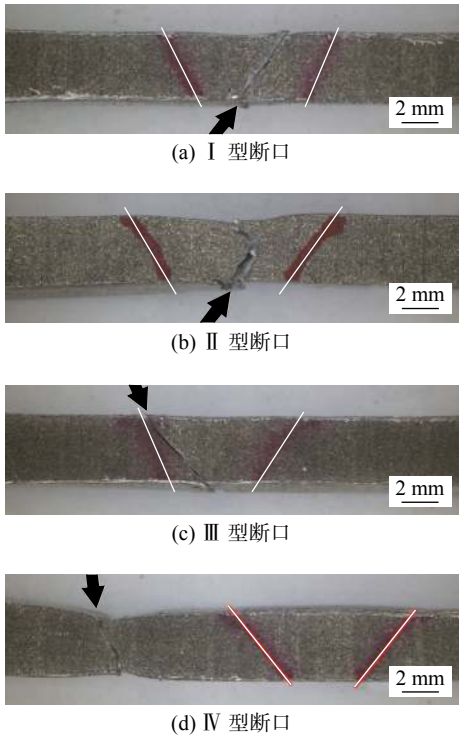

(a) Ⅰ 型断口

(b) Ⅱ 型断口

(c) Ⅲ 型断口

(d) Ⅳ 型断口

图 10　焊接接头拉伸断口宏观形貌

Fig. 10　Macro morphologies of tensile fracture of welded joints. (a) type Ⅰ; (b) type Ⅱ; (c) type Ⅲ; (d) type Ⅳ

缝区的强度和塑性较低. 当引入超声电弧后, 断口类型主要为Ⅰ型、Ⅳ型, 因为超声的存在使胞状树枝晶的尺寸变小、数量减少, 等轴晶区域的面积增加, 焊缝气孔量减少, 焊缝有效承载面积增加, 所以焊缝区的强度有明显的提升, 当焊缝区的承载强度超过热影响区中软化区的强度时, 试样将会在热影响区断裂, 所以加入超声电弧后, 断口类型除了Ⅰ型外主要为Ⅳ型. 接头的拉伸性能受焊缝气孔、显微组织、热影响区软化的综合影响. 超声激励频率为 70 kHz 时, 也出现了Ⅱ型断口, 这与焊缝组织中出现的柱状亚晶有关. 对于断后伸长率, 它的变化趋势与焊缝气孔率的相关性较大, 焊缝的气孔数量越少, 对应的断后伸长率越大.

图 11 为常规 MIG 焊和 50 kHz 时超声电弧 MIG 焊接头断口微观形貌. 在拉伸应力的作用下, 材料微区发生塑性变形, 在应力集中处或气孔缺陷处, 显微孔隙形核、长大、聚集, 断裂后形成了韧窝, 韧窝底部可见第二相粒子. 常规 MIG 焊断口中的韧窝尺寸较大, 大小、深浅不均匀, 并存在撕裂的痕迹, 所以强度和塑性都较低. 当引入超声电弧后, 断口为较小且均匀的等轴韧窝, 深度较大, 接头强度和塑性都得到提升.

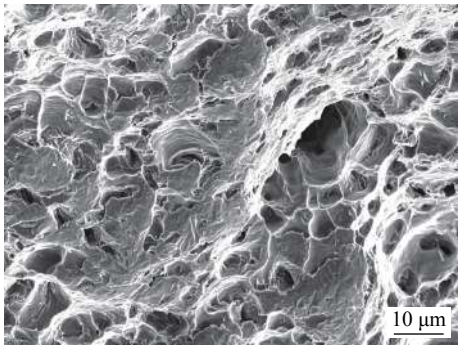

(a) 未施加超声电弧

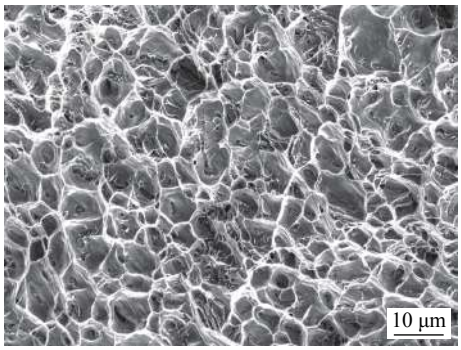

(b) 加入 50 kHz 的超声电弧

图 11 接头拉伸断口的微观形貌

Fig. 11 Tensile fracture micro-morphologies of welded joints. (a) without arc-ultrasonic treatment; (b) with arc-ultrasonic treatment of 50 kHz

3 结论

(1) 与常规 MIG 焊接头相比, 超声电弧的引入使焊缝中下部的熔宽显著增加, 使焊缝气孔量减少, 激励频率越大, 气孔量越少.

(2) 超声电弧可细化焊缝中部的胞状树枝晶组织, 增加等轴晶区域的面积, 在激励频率为 30 和 50 kHz 时较为明显. 而激励频率增加到 70 kHz 时, 焊缝中部组织中新出现了部分柱状亚晶.

(3) 加入超声电弧后, 由于焊缝中气孔和粗大胞状枝晶减少, 接头强度和塑性提升, 在激励频率为 50 kHz 时, 接头的抗拉强度最高, 达到 235 MPa, 为母材强度的 73.4%, 相比常规 MIG 焊接头提升了 6.6%. 断后伸长率随着激励频率增加而增加.

参考文献

[1] Tisza M, Lukács Zs. High strength aluminum alloys in car manufacturing[J]. IOP Conference Series: Materials Science and Engineering, 2018, 418(1): 1 − 8.

[2] 董晓晶, 李桓, 杨立军, 等. 铝合金多股复合焊丝脉冲 MIG 焊接接头组织与性能分析 [J]. 焊接学报, 2019, 40(11): 61 − 67.
Dong Xiaojing, Li Huan, Yang Lijun, *et al*. Microstructure and mechanical properties of pulse MIG aluminum alloy welded joints by means of a novel multistrands composite welding wire[J]. Transactions of the China Welding Institution, 2019, 40(11): 61 − 67.

[3] Lei Y, Xue H, Hu W, *et al*. Effect of arc ultrasonic vibration on microstructure of joint of plasma arc 'in situ' welding of SiC_p/6061 Al[J]. Science and Technology of Welding and Joining, 2011, 16(6): 561 − 566.

[4] 雷玉成, 罗雅, 任丹, 等. 微量 CO_2 对 MGH956 合金超声电弧 TIG 焊的影响 [J]. 焊接学报, 2014, 35(9): 1 − 5, 7.
Lei Yucheng, Luo Ya, Ren Dan, *et al*. Effect of trace CO_2 on arc-ultrasonic TIG welding of MGH956 alloy[J]. Transactions of the China Welding Institution, 2014, 35(9): 1 − 5, 7.

[5] 沈旭. 镀锌钢板超声-MIG 复合焊接成型研究 [D]. 南昌: 南昌大学, 2018.

[6] Kang Yuqing, Shen Haoran, Fu Yang, *et al*. Microstructure evolution and mechanical properties of the Sip/Zn-Al composite joints by ultrasonic-assisted soldering in air[J]. China Welding, 2018, 27(2): 39 − 44.

[7] Zhang Yanjun, Wu Minsheng, Li Luming, *et al*. Improving weld quality of 09MnNiDR steel by using arc-excited ultrasonic[J]. China Welding, 2006, 15(1): 6 − 10.

[8] 罗雅, 雷玉成, 黄巍, 等. 电弧超声激励频率对 MGH956 合金 TIG 焊接头的影响 [J]. 材料科学与工艺, 2014, 22(5): 26 − 30.
Luo Ya, Lei Yucheng, Huang Wei, *et al*. Effect of arc-ultrasonic excitation frequency on the properties of MGH956 alloy joint with TIG welding[J]. Materials Science & Technology, 2014, 22(5): 26 − 30.

[9] Wang Gui, Dargusch M S, Qian M, *et al*. The role of ultrasonic treatment in refining the as-cast grain structure during the solidification of an Al–2Cu alloy[J]. Journal of Crystal Growth, 2014, 408: 119 − 124.

[10] Jian Xiaogang, Meek T T, Xu Hanbing, *et al*. Degassing of molten aluminum A356 alloy using ultrasonic vibration[J]. Materials Letters, 2004, 58(29): 3669 − 3673.

第一作者简介: 雷玉成, 1962 年出生, 博士, 教授; 主要研究方向为先进连接方法、焊接过程控制和模拟; 发表论文 150 余篇; Email: yclei@ujs.edu.cn.

(编辑: 孙焕焕)

Yicheng[1], XU Yinan[1], ZHOU Kun[1] (1. Harbin Welding Institute Co., Ltd., Harbin, 150028, China; 2. China Academy of Machinery Science and Technology Group Co., Ltd., Beijing, 100044, China; 3. University of Science and Technology Beijng, Beijing, 100083, China). pp 18-23

Abstract: By stainless steel welding wire with different Si element content, the weld forming, microstructure and performance after high-speed welding has been organized for research purposes, with the GMAW welding method,by analysis means of SEM, XRD diffraction pattern, mechanical properties such as stretching and the micro hardness testing, to further study of Si elements in the weld internal space distribution, and its influnce rule on microstructure,mechanical properties when forming after welding. The results show that the specific content of Si element in the welding wire can not only increase the metal fluidity in the weld pool, but also improve the stability of the welding process and the weld forming after welding. At the same time, the welding speed can be greatly increased to 120 cm/min; As a result of the existence of element Si, the joint organization after GMAW high-speed welding mainly austenite and δferrite, weld organization optimized. In XRD diffraction pattern after welding, martensite and cementite exists in the joint organization, micro hardness increased, tensile properties are basic flat, and apparent necking have appeared in front of the tensile fracture, plasticity and tensile strength are good.

Key words: alloy element Si; welding speed; organizations; hardness; tensile property

Study on the application of the weld reinforcement variation coefficient in underwater wet welding quality evaluation DU Yongpeng[1,3], GUO Ning[1,2], WU Chenghao[1,2], HUANG Lu[1,2], ZHANG Xin[1,2], FENG Jicai[1,2] (1. Shandong Provincial Key Laboratory of Special Welding Technology, Harbin Institute of Technology at Weihai, Weihai, 264209, China; 2. State Key Laboratory of Advanced Welding and Joining, Harbin Institute of Technology, Harbin, 150001, China; 3. Institute of Ocean graphic Instrumentation, Shandong Academy of Science, Qingdao, 266001, China). pp 24-27,32

Abstract: There is a lack of an evaluation index which can assess the appearance of welds user-friendly and accurately in underwater wet welding. To solve this problem, the weld reinforcement variation coefficient is proposed to be used for evaluating the welding quality. The evaluation index has many advantages such as objective, quantitative, less step and easy operation, which is suitable for popularization and application in practical engineering production. The weld reinforcement variation coefficient grows higher with the worse the uniformity of weld appearance and the lower the welding quality and vice versa. According to the influence of pulse current on the stability of welding process, welding was carried out under different pulse frequency conditions. In view of the influence of wire feeding method on welding process, the stability of underwater wet flux-cored wire welding process was studied by analyzing the wire feeding method with the coefficient of variation of residual high welding seam. The experimental results show that the evaluation results of the index have high consistency with welding quality. The influences of the welding process on the weld reinforcement variation coefficient are analyzed using an X-ray transmission method. The reliability of the weld reinforcement variation coefficient is further verified by researching the welding electrical signal and droplet transfer.

Key words: underwater wet welding; welding quality; weld reinforcement; variation coefficient

Anti-aging performance of Sn5Sb1Cu0.1Ni0.1Ag/Ni solder joints SUN Fenglian, LI Tianhui, HAN Bangyao (Harbin University of Science and Technology, Harbin, 150040, China). pp 28-32

Abstract: In this paper, SEM was used to study the interfacial diffusion behavior of Cu/Sn5Sb1Cu0.1Ni0.1Ag/Cu and Ni/Sn5Sb1Cu0.1Ni0.1Ag/Ni solder joints under isothermal aging at 150 ℃. The results showed that the morphology of intermetallic compound (IMC) at Cu/Sn5Sb1Cu0.1Ni0.1Ag/Cu solder joint grew from thin needle-shaped to rod-shaped and the thickness of IMC increased with aging time increasing. The main composition of IMC was $(Cu,Ni)_6Sn_5$. The appearance of IMC at Ni/Sn5Sb1Cu0.1Ni0.1Ag/Ni solder joints changed from horst shaped to relatively granular shaped, and the thickness of IMC increased. The main composition of IMC was $(Cu,Ni)_3Sn_4$. The growth rate of IMC at interface of Sn5Sb1Cu0.1Ni0.1Ag/Cu solder joint was 7.39×10^{-2} μm^2/h, and that at interface of Sn5Sb1Cu0.1Ni0.1Ag/Ni was 2.06×10^{-2} μm^2/h. Nickel-plating significantly changed the morphology of IMC, reduced the growth rate of IMC, inhibited the growth of IMC, and significantly improved the aging resistance.

Key words: Sn5Sb1Cu0.1Ni0.1Ag; IMC; isothermal aging; nickel-plating

Effect of arc-ultrasonic on the microstructure and properties of 6061 aluminum alloy joint with MIG welding LEI Yucheng[1], CUI Zhanxiang[1], LU Guangyao[2], YAO Yiqiang[2], ZHANG Xuening[1] (1. Jiangsu University, Zhenjiang, 212013, China; 2. China General Nuclear Power Corporation, Shenzhen, 518000, China). pp 33-38

Abstract: To improve the quality of MIG welded joints of aluminum alloys, the ultrasonics were generated in the MIG welding arc with external ultrasonic excitation source, and the influence of the excitation frequency on the weld appearance, pore distribution, microstructure and mechanical properties of the 6061-T6 aluminum alloy butt weld was studied. The results show that arc-ultrasonic can effectively refine the microstructure of weld metal, reduce pores in the weld, and increase the strength of the welded joints. Compared with conventional MIG welding, arc-ultrasonic technique can increase the weld width, refine the cellular dendritic and enlarge the equiaxed grain zones in the weld metal. Microstructure refinement efficiency is most excellent when the excitation frequency is 30 kHz. As the excitation frequency increases, the number of pores in the weld gradually decreases, and the tensile strength of the joint is improved. The maximum tensile strength is 235 MPa, which is 73.4% of the base metal under the excitation frequency of 50 kHz, and accordingly the dimples in the tensile fracture have a more equiaxed shape and a more homogenized distribution.

Key words: arc-ultrasonic; excitation frequency; microstructure; tensile strength; 6061 aluminum alloy

Vacuum brazing diamond process under the profile constraint and analysis of agreed height abrasives HE Qingshan[1], CUI Zhongming[1], FU Yucan[2], WANG Zhixin[3] (1. Henan University of Technology, Zhengzhou, 450001, China; 2. Nanjing University of Aeronautics and Astronautics, Nanjing, 210016, China; 3. National-Local Union Engineering Laboratory of High Efficiency Precision Diamond Cutting Tool Technology, Zhongyuan University of Technology, Zhengzhou, 450007, China). pp 39-42

Abstract: The brazing experiments in vacuum furnace were carried by a special method of keeping diamond within the bounds of graphite template, which realized a high bonding strength between steel matrix and diamond and an effective way to control agreed height abrasives. Welded joints and morphology of diamond surface were observed by SEM. Fixed-point and micro-region compositions on the diamond surface were analyzed by EDS. The agreed height abrasives were measured by super-field 3D microscope. Results show that liquefied Cu70Sn20Ti10 solder under capillary action can infiltrate and enclose diamond on the profile of graphite template through splicing and steel matrix have a high holding power for diamond due to the formed TiC on bonding interfaces. Silver colloid and diamond can't generate reaction during brazing process. As silver colloid can always have good bonding and constraint effect for diamond, agreed height of abrasives is satisfactory after brazing process.

Key words: brazing; profile constraint; diamond; agreed height abrasives

Mechanism of weld formation using double pulsed variable polarity plasma arc welding of high strength aluminum alloy DU Maohua, HAN Yongquan, FAN Weijie, HONG Haitao (Key Laboratory of Material Forming, Inner Mongolia University of Technology, Hohhot, 010051,China). pp 43-47

Abstract: By setting up a double pulse variable polarity plasma arc welding system, through process test of high strength aluminum alloy welding with double pulse VPPA (variable polarity plasma arc), weld formation and mechanical properties of welded joints of low frequency pulse modulation superposition high frequency pulse were studied. The results show that the low frequency pulse can obtain the fish scales weld by the periodic oscillating liquid molten pool. The high frequency pulse causes the arc more concentrated and improves effectively the energy density of the arc, thus enhance the arc force. Coupled oscillation of the double pulse strengthen the stirring of the molten pool, and refine the grain sizes of the aluminum alloy weld. The tensile strength of welded joints reaches 384.13 MPa, compared with VPPA welded joints, the strength is increased by about 10.21%. And the percentage reduction of area and percentage elongation of welded joints have been improved to a certain degree. The double pulse VPPA welding process improves the mechanical properties of the welded joints of the aluminum alloy.

Key words: variable polarity waveform; pulse modulation; weld formation

Detection of weld defects based on FGT - FBP reconstruction algorithm ZHOU Xiaohu, GAO Xiangdong, DU Liangliang, WANG Chuncao (Guangdong Provincial Welding Engineering Technology Research Center, Guangdong University of Technology, Guangzhou, 510006, China). pp 48-52

Abstract: An innovative detection method based upon fuzzy gray scale transformation and filter back-projection (FGT-FBP) reconstruction is proposed to study the geometrical characteristics of weld defects. By analyzing the characteristics of magneto-optical images with defects such as cracks and incomplete penetration under alternating magnetic field excitation, a fuzzy rule is designed to carry on fuzzy gray scale transformation of the magneto-optical image. The image contrast is improved to visualize the configuration and trend of weld defects. An image evaluation method without reference models that describes weld defect details of magneto-optical images is realized. The weld defect magneto-optical images processed by FGT are rotated and projected. Fast Fourier